ORIGINAL PAPER

Triptan partition in model membranes

Irene Wood · Mónica Pickholz

Abstract In this work, we report a molecular dynamics simulations study of protonated triptans, sumatriptan and naratriptan, in a fully hydrated bilayer of 1-palmitoyl-2-oleoyl-*sn*-glycero-3-phosphatidyl-choline (POPC). The simulations were carried out at two concentrations for each drug. Our results show partition between the lipid head-water interphase and water phase for both triptans, with increasing access to the water phase with increasing concentrations. The triptans were stabilized at the interphase through different specific interactions with the POPC bilayer such as hydrogen bonds, salt bridges, and cation-π. Besides, sumatriptan and naratriptan protonated molecules have no access to the hydrophobic region of the bilayer at the studied conditions. Similar results were found for both drugs, however protonated naratriptan shows slightly higher affinity for the water phase. This behavior was attributed to the bulky lateral amino group in its structure under the studied conditions (drugs were originally placed at the water phase). This work represents a first insight to the comprehensive understanding of triptan partition in model membranes.

I. Wood · M. Pickholz
Departamento de Tecnología Farmacéutica, Facultad de Farmacia y Bioquímica, Universidad de Buenos Aires, Junín 956, Buenos Aires CP1113, Argentina

M. Pickholz (✉)
Instituto Nanobiotec, Consejo Nacional de Investigaciones Científicas y Técnica (CONICET), Rivadavia 1917, Buenos Aires CP1033, Argentina
e-mail: mpickholz@gmail.com

Introduction

Migraine is a multifactorial syndrome characterized by headache, nausea, vomiting, sensitivity to light, noise, and movement [1]. In a general way, the neurovascular headache is caused by neural events leading to vasodilatation, pain, and increase of neuronal activation [2].

The association of the neurotransmitter serotonin (5-hydroxytryptamine, 5-HT) with migraine is due to several findings such as sudden 5-HT release, as a trigger event and increased urinary excretion of its main metabolite, during attacks [3]. In this way, the development of anti-migraine pharmacology was directed to the serotonin receptor subclass 5-HT-1_B [4], located mostly in cranial vessels [5] and some nerves [6].

The triptan prototype, sumatriptan (SMT), was designed based on the 5-HT structure and represents a valuable tool to understand the pathophysiology of migraine and 5-HT role [6–8]. SMT was proposed as a vasoconstrictor agent on cranial blood vessels [4, 6, 7, 9–13]. In addition, SMT blocks neurogenic inflammation and nociception in the central nervous system (CNS) [2, 4, 12, 14, 15]. SMT has selective activity of some 5-HT1 and is essentially inactive on other receptors [2, 4, 6, 9]. A new family of triptans was developed, looking for improved SMT properties [16]. The triptans available show affinity for 5-HT receptor 1_B, 1_D and most of them also for 1_F [13]. In this context, naratriptan (NRT) has emerged to treat patients who respond poorly to oral SMT [17], seeking for greater metabolic stability and oral bioavailability [18]. It is suggested that NRT is slightly more lipophilic [19]. Besides, in comparison with SMT, NRT shows more noticeable central action, lower absolute dose, slower onset of action, lower recurrence rate and increased plasma half-life [8, 14, 19, 20].

The correlation between the triptan effectiveness and their ability to cross blood–brain barrier (BBB) still unknown, in

our knowledge. A good brain penetration can have somehow contradictory effects: increase efficiency — action on central receptors — and reduce safety [19]. In particular, most authors proposed that SMT has peripheral action because it does not easily pass BBB under normal circumstances [7]. Nevertheless, BBB could be altered during migraine attacks [4, 7, 19, 21], helping SMT penetration. Some central adverse effects observed after SMT administration could be explained considering this alteration [6, 21]. Among the triptan family, NRT was developed looking for access to CNS [19], allowing its preventive use [8, 18]. However, experimentally measured brain penetrability for NRT was no higher than for SMT [18].

We have recently used molecular dynamics simulations to study interactions between protonated sumatriptan and 1-palmitoyl-2-oleoyl-*sn*-glycero-3-phosphatidylcholine (POPC) bilayers [22]. The simulations were carried out as a function of the sumatriptan concentration. This study shed light on the main interactions responsible for the distribution of the drug within the bilayer. In the present work, we extend our study in order to compare the effects off two different triptans — SMT and NRT — in their main interactions with lipid bilayers at different concentrations. Since SMT and NRT pKa values are 9.63 [23, 24] and 9.70 [25], respectively, the prevalent ionization forms at relevant pH is the protonated one. At physiological pH, considering Henderson-Hasselbach equation, 99.3 % of SMT molecules are charged and 98.4 % for NRT. In this way, we focus our attention on the protonated form of these drugs. Nevertheless, the importance of the neutral specie cannot completely be neglected and we will address this point in the near future. Besides, model membranes of POPC were chosen because phosphatidylcholine lipid types are the most abundant among mammal endothelial cell membranes [26]. POPC bilayers could be used as an accurate system to study permeation of several molecules and drugs, as a model of BBB [27].

In the next sections, we discuss the methodologies applied, followed by the results and discussion.

Systems and simulation details

We have studied the protonated sumatriptan (pSMT) and naratriptan (pNRT) interactions with a POPC phospholipid bilayer through molecular dynamics simulations. The simulations were performed using the NAMD2 program [28] within the CHARMM force field [29]. The water molecules were described by the TIP3P model [30]. The drug containing bilayers were built using *Packmol* package [31].

In Fig. 1a and b we show the molecular structure of pSMT and pNRT, respectively. Looking at these molecules, we can see similarities and differences in their structures. Both drugs share the indole skeleton bi-substituted in the same positions as serotonin and other related molecules [32]. The substitution at the
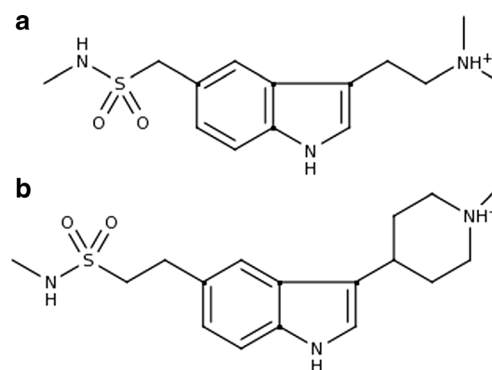

Fig. 1 Structures of protonated drugs: **a** Sumatriptan (*pSMT*) and **b** Naratriptan (*pNRT*)

five-membered ring is an aliphatic amino group protonated at physiological and low pH: di-methyl-amino-ethyl group for pSMT and methyl-piperidine for pNRT. The substitution at the six-membered ring is a N-methyl sulfonamide group linked by methylene in pSMT and by ethylene in pNRT. The parameterization for pNRT was based on the CHARMM force field and quantum chemical calculations, as done for pSMT [22]. All drugs were considered fully flexibles. The force constants were chosen in analogy to similar molecules. The intra-molecular bond lengths and angles on the equilibrium geometry were optimized using the density functional theory (DFT) with the B3LYP [33] functional and 6-311G** basis set. The partial atomic charges were obtained from a single point HF/6-31G* calculation, using the Gaussian03W package [34], and the Merz–Singh–Kollman protocol [35]. Both, optimization and partial charges calculations were performed using the polarized continuum model (PCM) [36] with a solvent dielectric constant of 80, corresponding to liquid water at room conditions. In our previous work [32], PCM method was needed in order to obtain the zwitterionic charge separation of the tryptophan amino acid. Here, in order to compare with this work, we have chosen the same methodology.

All simulated systems studied here consist of a lipid bilayer containing 150 POPC molecules (75 in each leaflet) fully hydrated. We have carried out two series of simulations for each of the drug, at two different drug:lipid ratio: 1:75 (low concentration) and 1:3 (high concentration). The drugs were initially placed in the water phase. The number of water molecules on the simulation box was 4200 and 5000 for low and high concentrations, respectively. In order to assure electro neutrality we added chloride counter ions for each of the protonated drugs.

Classical atomistic MDs were performed at the NPT conditions. The temperature was maintained constant at 310 K, by means of a Langevin thermostat by applying friction and random force [28]. The Langevin thermostat was used without coupling to hydrogens and with a damping coefficient of 1/ps. Besides, pressure was maintained at 1 atm by using a Langevin barostat [37, 38] with a piston period of 5 ps and a damping time of 5 ps.

The simulation box was fully flexible. A multiple-time step algorithm, RESPA [39], was used with the shortest time step of 2 fs. The short-range forces were computed using a cut-off of 10 Å and the long-range forces were taken into account by means of the particle mesh Ewald (PME) technique [40]. Additionally, periodic boundary conditions were considered. The simulations were run up to 100 ns.

Simulation results

In this section, we discuss the main results of our study. For the statistical analysis of most of the properties, we have just considered the last 50 ns of the simulation trajectories.

The interfacial ordering of the systems was evaluated by means the electron density profile (EDP) normal to the bilayer (z coordinate); z=0Å corresponds to the membrane center. In Fig. 2, we show the EDPs for low and high concentrations. The POPCs bilayers are shown in black, water in blue and pSMT in red and pNRT in green. pSMT and pNRT were magnified ten times for low concentration cases, for visualization purposes. As an overall picture, we can see from these figures that triptans essentially show partition between the water phase and the lipid head-water interphase, with no access to the hydrophobic tail region for both drugs. Differences between pNRT and pSMT are not evident. Comparison between drugs shows a higher access of pNRT to the water phase. In this way we can see an imbalance between leaflets for this molecule at low concentrations. It is important to point out here, that drugs cross from one monolayer to the other just through the water phase. In order to illustrate that, in Fig. 3a and b we show the center of mass drug's trajectories of

each pSMT and pNRT, respectively, over the last 50 ns of the simulation runs. While in Fig. 2 the distributions are centered in the middle of the lipid bilayer, in Fig. 3 z=0Å corresponds to the center of the water phase (taking into account the periodic boundary conditions). This condition could be compared against multilamellar vesicle, since the amount of water was estimated for a fully hydrated lipid bilayer [41]. We can see from these figures that, in both cases, molecules have access to the water phase and the crosses from one monolayer to the other happen through the water phase (see black curves). Similar results are obtained for the high concentrations cases.

Following our previous work [22], we have estimated the percentage of the pNRT in water phase. The percentage of pNRT was estimated as 25 % and 73 % for low and high concentrations, respectively. These values are considerable higher than the already reported 20 % and 63 % for pSMT [22]. A rough estimation of the free energies of partition between the water and membrane phase could be made through the equation $\Delta\Delta G_{w–m}=-KT \ln (C_w/C_m)$ [42], where C_w and C_m are the drug average concentrations at the water and membrane phases, respectively. The calculated values are 3.4 ± 0.4 and 2.7 ± 0.4 kJ mol^{-1} units for pSMT and pNRT at low concentrations. At high concentrations we found that the free energies change sign, (-1.4 ± 0.3 kJ mol^{-1} pSMT and-2.5 ± 0.3 kJ mol^{-1} pNRT) showing a higher affinity for the water phase than for the interphase.

Furthermore, the effects of both triptans on the average area per lipid are negligible. The main effects were found for the pSMT case at high concentration where the area per lipid slightly increased from 59.0 Å^2 (plain bilayer and low concentrations) to 60.7 Å^2.

Fig. 2 Electron density profile (*EDP*) of the different systems. Water densities and POPC are depicted in blue and black, respectively (pSMT systems in full lines, pNRT systems in dotted lines). pSMT and pNRT densities are depicted in red and green, respectively. Panel A corresponds to low drug concentration (*1:75*) and panel B to high concentration (*1:3*). Drug densities in panel A are magnified tenfold for easy visualization. z=0 corresponds to bilayer center
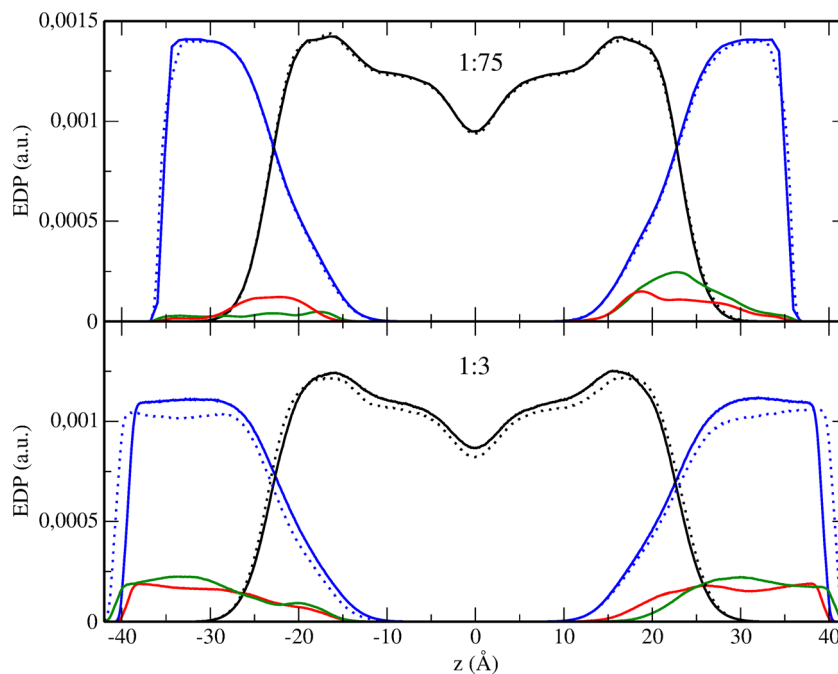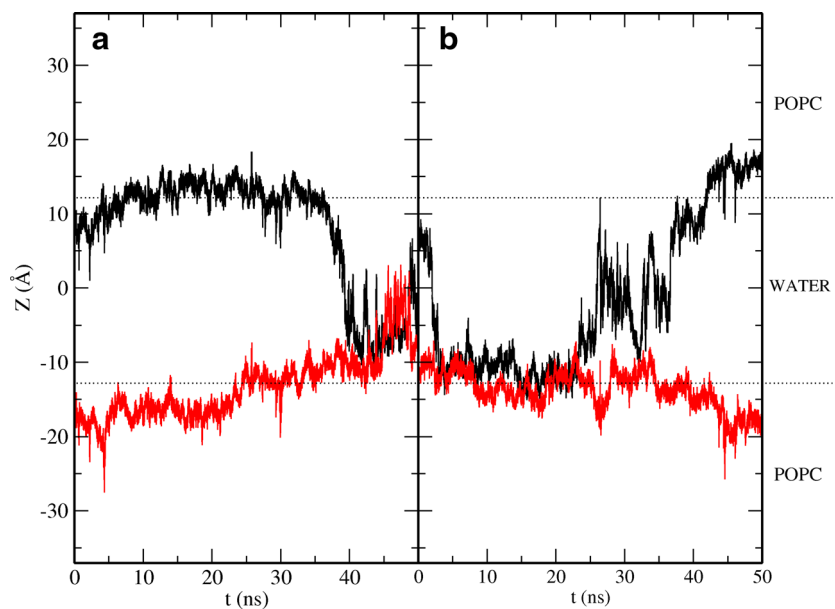
Fig. 3 Water centered trajectories along the z axes of the center of mass of triptans at low drug concentration (*1:75*). The separated residues of both drugs are depicted in black and red for easy visualization. Panel A corresponds to pSMT and panel B to pNRT

In order to analyze the triptan effects on the bilayer polarization, we computed the electrostatic potential across the interphase by evaluating the double integral of the charge density [43] for the POPC lipid bilayers. The charged profiles were averaged over the two monolayers. In Fig. 4 we show the results for pNRT and pSMT at high concentration. There was almost no effect of pNRT on the polarization effects of the POPC lipid bilayer, when compared with the plain bilayer. However, the presence of pSMT at high concentration causes a noticeable increase on the POPC potential (~0.10 V) (data not shown).

As we have discussed in previous works [22, 32] the main interactions that stabilize indole related molecules are cation–π, salt bridges, and hydrogen bond interactions.

The cation–π interaction is essentially driven by electrostatic attraction between cations and the negative face of conjugated rings [44]. Through this type of interaction, indolic molecules, such as serotonin and precursors, adopt an interfacial location in lipid bilayers [32]. In particular, aromatic compounds, such as serotonin, SMT and NRT, are electrically characterized by its quadrupolar moment and act like a π-donor interacting with the choline (the positively charged amino group of POPC). The radial distribution function, $g_{c-\pi}(r)$, between the pSMT and pNRT centroid of the benzene ring of indole and charged nitrogen (N) atom of choline in POPC could be used as an estimation of the distance condition for this kind of interaction [45]. In Fig. 5 we show the calculated $g_{c-\pi}(r)$ functions for both triptans at low (dashed lines) and high (solid lines) concentrations. We can see a
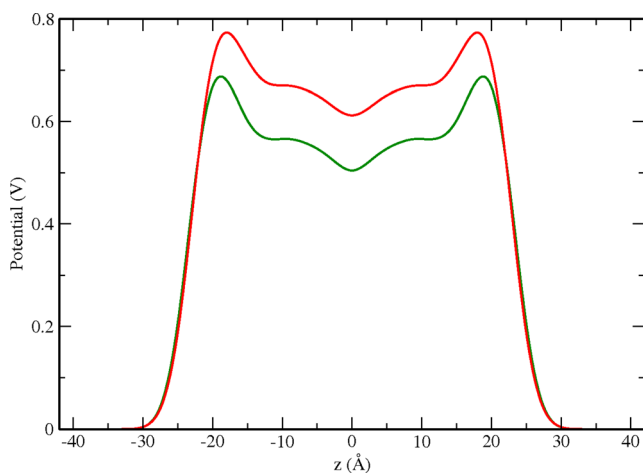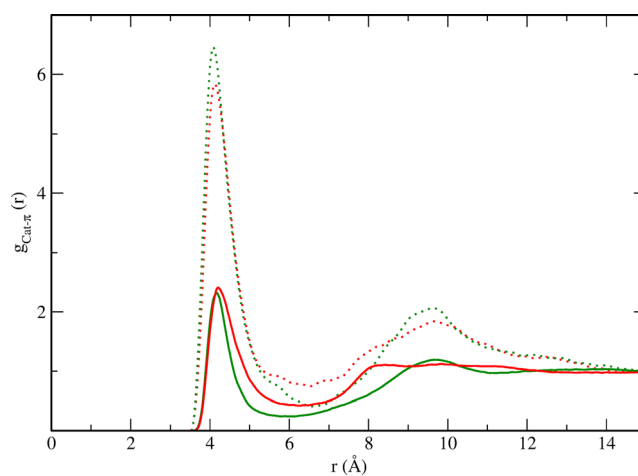

Fig. 4 Overlapping of POPC electrostatic potentials for high drug concentration (*1:3*). pSMT and pNRT are depicted in red and green, respectively. z=0 corresponds to bilayer center

Fig. 5 Radial distribution function between the benzene centroid of triptan and charged choline group of POPC. pSMT and pNRT are depicted in red and green, respectively. Dotted lines correspond to low drug concentration (*1:75*) and full lines to high concentration (*1:3*)

well-defined peak at ~4.0 Å for the four cases. The behavior is quite similar between triptans as a function of the concentration. In particular, we can see that the first peak drops in intensity at high concentrations due to increased partition at the water phase. This effect is more pronounced for pNRT.

The number of HB established by a selected pair was determined by averaging over the simulation run time and the number of pairs that satisfy the geometric criteria — distance between the acceptor, and a hydrogen atom should be shorter than or equal to 2.0 Å and the angle between donor-hydrogen-acceptor should be smaller than 30°. Since POPC can act just as an acceptor through the non-ester oxygen atoms of phosphate (Op) and carbonyl (Oc) groups—oxygen atoms that are just bonded to one heteroatom—we calculated the number of HB between them and the three donor groups (lateral amino, NH indole, and NH sulfonamide) for both triptans. Since HB formation with the POPCs Oc is considerably low for all the considered concentrations, as follows, we will discuss the different HB interactions with the POPCs Op. In Table 1, we show the average number of HB between NH groups the triptans and Op (POPC). In order to facilitate the comparison we show the estimated number of HB per molecule at the interphase.

NH sulfonamide As we can see from the table, the number of HB at the interphase increases with concentration for both triptans (49 % and 25 % for pSMT and pNRT, respectively). Furthermore, pNRT more strongly interacts with Op through the sulfonamide group than pSMT. It is important to point out here that the sulfonamide's pNRT has an extra methylene group linked to the indole ring that increases its flexibility with respect to pSMT.

NH indole The interaction between these groups was found to oppositely affect the triptans. While for pNRT the number of HB per molecule at the interphase was considerably reduced (from 0.6 to 0.3) when the concentration increased, for pSMT it was increased from 0.3 to 0.4. Furthermore, comparing both triptans at the same concentrations we found that this interaction is stronger for pNRT at low concentrations and it is inverted at high concentrations.

Lateral amino The stronger interaction with this group was found for the pSMT at low concentration (0.7HB). Even if

pNRT forms essentially half of the hydrogen bonds at low concentration, both drugs show similar behavior at high concentrations (~0.4HB per molecule at the interphase). We found somehow a complementary result than the one found for the NH indole ring.

In addition, we have investigated the salt bridge (SB) interaction between the drugs and the bilayer. SB is a non-covalent electrostatic interaction established between oppositely charged pairs [46–48]. The SBs between N atom of lateral amino group (pSMT, pNRT) and P atom of phosphate group (POPC) were investigated through the radial distribution function, $g_{SB}(r)$, analysis. In Fig. 6 we show the $g_{SB}(r)$ for the studied conditions. In this figure we observe two well defined peaks at ~4.0 Å and ~4.7 Å for pSMT and at ~3.8 Å and ~5.3 Å for pNRT, as evidence of the SB formation. The first peak was slowly shifted (~0.2 Å) for both concentrations. Besides, the peaks at 4.7 Å and 5.3 Å were also shifted. These effects were essentially due to different steric effects caused by different groups substituting the charged amino group in both drugs: the methyl and ethyl groups in pSMT and the methyl and aliphatic ring groups in pNRT. Effects such as chemical environment and steric features contribute to the strength of the interaction. Comparing both molecules, pSMT shows more enhanced SB interaction than pNRT as concentration rises, in agreement with HB interactions (Table 1).

The differences in peak intensities between pSMT and pNRT could be attributed to different localization in the bilayer. In this way, we have analyzed density distribution of different triptan groups. As we already discussed, the triptans at the higher concentration, are distributed between water and interphase. Most of the groups are superposed at the same region, showing in average no preferential orientation. However, as we can see in Fig. 7, where the EDPs of the amino lateral groups are shown, we can see a noticeable difference between drugs. For pNRT, the lateral NH group has less access to the interphase than for pSMT, affecting interactions with POPC head groups as SB. Keeping in mind that triptans were originally placed in the water phase, the entrance of pNRT seems to be more hindered by the bulky aliphatic ring.

In order to summarize this work in a visual way, we show in Fig. 8 a snapshot of the bilayer containing the drugs (NRT at high concentrations), along with zoom illustrating two of their main interactions: cation-π and salt bridge.

Table 1 Number of hydrogen bond (*HB*) interactions performed per residue in interphase between different amino groups of triptans and oxygen atoms of POPC phosphate group. Statistical errors are shown in brackets

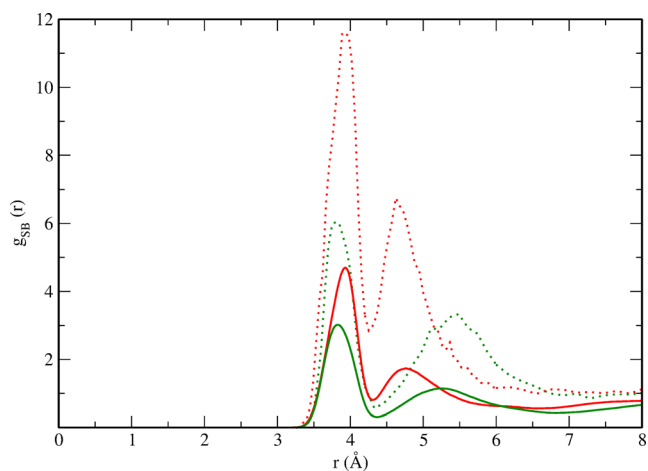| Drug:POPC ratio	Drug	Lateral (NHlat)	Indole (NHind)	Sulfonamide (NHsulf)
		mean (error)	mean (error)	mean (error)
Low (1:75)	pSMT	0.769(3)	0.314(3)	0.285(2)
	pNRT	0.339(2)	0.615(3)	0.485(3)
High (1:3)	pSMT	0.463(1)	0.430(1)	0.426(1)
	pNRT	0.415(1)	0.328(1)	0.605(1)

Fig. 6 Radial distribution function between the charged lateral amino group of triptan and the phosphate group of POPC. pSMT and pNRT are depicted in red and green, respectively. Dotted lines correspond to low drug concentration (*1:75*) and full lines to high concentration (*1:3*)

Conclusions

MD simulations were performed in order to compare the effects of two protonated triptans (anti-migraine drugs), in their interaction with model membranes at different concentrations. Even though sumatriptan and naratriptan belong to the same family, and share some structural characteristics, they show different pharmacokinetic properties.

Our results show that pSMT and pNRT do not access the hydrophobic membrane region and interact essentially with lipid head groups and access to the water phase. The limitations of both triptans to cross membranes are essentially related to the presence of charged and anchoring groups interacting with water and head groups.
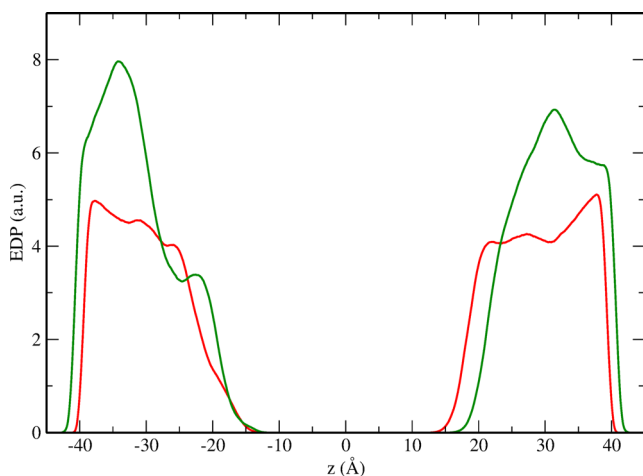

Fig. 7 Detailed electron density profile (*EDP*) of triptans lateral amino group at high drug concentration (*1:3*). pSMT and pNRT are depicted in red and green, respectively. z=0 corresponds to bilayer center
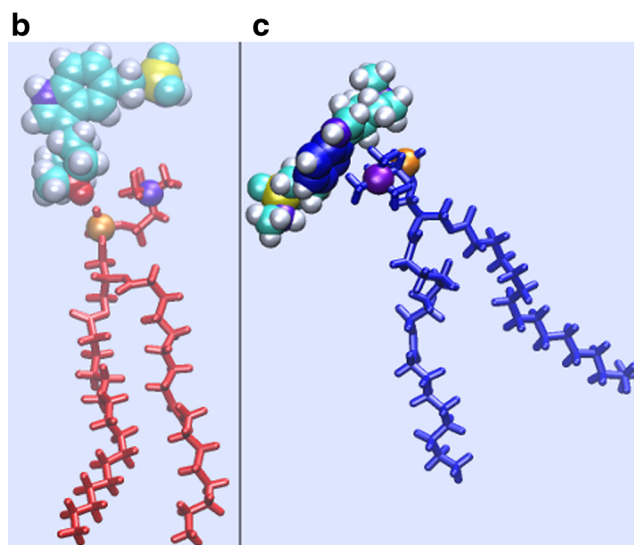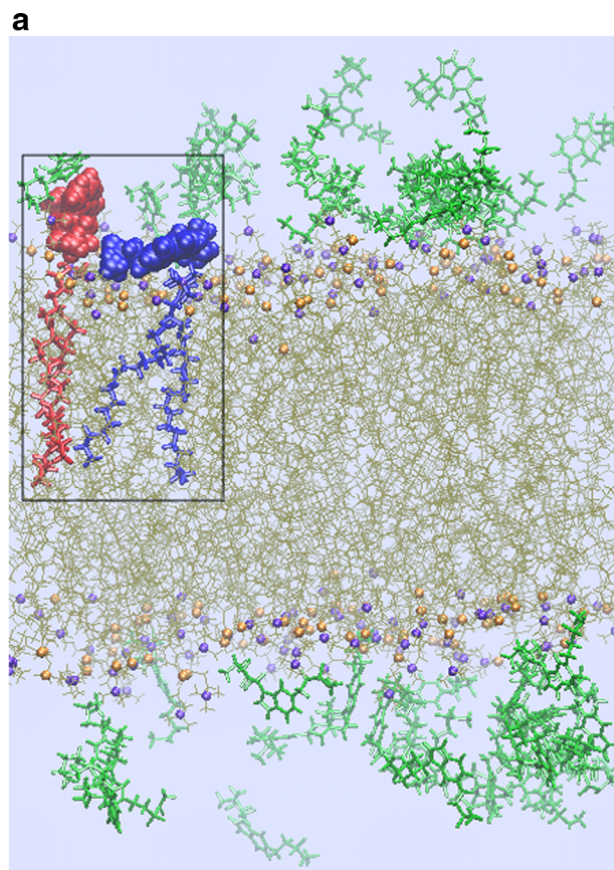

Fig. 8 **a** Snapshot of the bilayer containing pNRT, at high concentration: POPC lipids are shown in light brown (N and P atoms represented by violet and orange spheres, respectively) and pNRT in green. Water molecules were removed for visualization purposes. Besides, two pairs of lipids-pNRT were highlighted in blue and red respectively. A zoom of each of these pairs is shown, in order to exemplify a **b** salt bridge (*in red*) and a **c** cation-π (*in blue*) type of interactions. The figures were done using VMD 1.8.7 software package [50]

The same interfacial location of pSMT and pNRT came from their indole ring, as 5-HT: they are able to interact in a

similar way with lipid bilayers. The main specific interactions between pSMT or pNRT and lipid head groups are cation-π, salt bridges, and hydrogen bonds. These interactions depend both on drug and on concentration.

For instance, salt bridges formation between the lateral amino groups of the drugs and the POPCs phosphate is more pronounced for pSMT than for pNRT. This finding leads us to look more carefully to the distribution of the lateral amino groups. We found a noticeable difference between drugs. For naratriptan, this distribution is shifted to the water phase with respect to the sumatriptan, essentially for being a bulky aliphatic ring that precludes it to enter easily into the interphase. Besides preliminary results, where naratriptan was originally placed at the bilayer center (at the same concentrations), show higher drug partition on the membrane phase. However, sumatriptan distribution does not depend on initial conditions. Furthermore, both drugs have the same number of hydrogen bond donor (and acceptor) groups. They essentially differ in the flexibility of the sulfonamide group and the steric effects of the lateral amino group. We would like to summarize here that hydrogen bonds essentially form between the three amino groups of the drugs with the phosphate oxygens of POPCs for both triptans. Furthermore, even if the intensity of each contribution varies both with drug and concentration, the total interaction numbers per molecule at the interphase are similar.

It is reported in the literature a higher lipophilicity of naratriptan with respect to sumatriptan [17, 19]. However, the partition coefficient values are not significantly different between them [18, 49]. At the conditions studied here, the results show very similar partition between drugs, with a slight preference of sumatriptan for membrane phase. This study was a first step in trying to understand the partition of both triptans in model membranes. We obtained interesting results, as we already described. Nevertheless, many questions on the subject remain open. Further analysis should be done in order to obtain a more comprehensive view, such as ionization effects and initial conditions.

References

1. Langemark M, Olesen J, Poulsen DL, Bech P (1988) Clinical characterization of patients with chronic tension headache. Headache 28:590–596

2. Goadsby PJ, Lipton RB, Ferrari MD (2002) Migraine - current understanding and treatment. N Engl J Med 346:257–270

3. Hamel E (2007) Serotonin and migraine: biology and clinical implications. Cephalalgia 27:1295–1300

4. Goadsby PJ (2000) The pharmacology of headache. Prog Neurobiol 62:509–525

5. Humphrey PPA (2008) The discovery and development of the triptans, a major therapeutic breakthrough. Headache 48:685–687

6. Humphrey PPA, Feniuk W, Marriott AS, Tanner RJN, Jackson MR, Tucker ML (1991) Preclinical studies on the anti-migraine drug, sumatriptan. Eur Neurol 31:282–290

7. Kaube H, Hoskin KL, Goadsby PJ (1993) Inhibition by sumatriptan of central trigeminal neurons only after blood–brain barrier disruption. Br J Pharmacol 109:788–792

8. Cady RK (2001) Looking forward: the expanding utility of sumatriptan and naratriptan. Cephalalgia 21:35–38

9. Peroutka SJ (1990) Sumatriptan in acute migraine: pharmacology and review of world experience. Headache 30:554–560

10. Buzzi MG, Moskowitz MA, Peroutka SJ, Byun B (1991) Further characterization of the putative 5-HT receptor which mediates blockade of neurogenic plasma extravasation in rat dura mater. Br J Pharmacol 103:1421–1428

11. Humphrey PPA, Feniuk W, Perren MJ, Beresford IJM, Skingle M, Whalley ET (1990) The neuropharmacology of serotonin. Ann N Y Acad Sci 600:587–598

12. Humphrey PPA, Goadsby PJ (1994) Controversies in headache. The mode of action of sumatriptan is vascular? A debate. Cephalalgia 14:401–410

13. Saxena PR, Tfelt-Hansen P (2001) Success and failure of triptans. J Headache Pain 2:3–11

14. Bigal ME, Bordini CA, Antoniazzi AL, Speciali JG (2003) The triptan formulations. A critical evaluation. Arq Neuropsiquiatr 31:313–320

15. Dodick DW, Silberstein S, Dahlof CGH (2002) Is there a preferred triptan? Headache 42:1–7

16. Goadsby PJ (1998) 5-HT1B/1D agonists in migraine: comparative pharmacology and its therapeutic implications. CNS Drugs 10:271–286

17. Stark S, Spierings ELH, McNeal S, Putnam GP, Bolden-Watson CP, O'Quinn S (2000) Naratriptan efficacy in migraineurs who respond poorly to oral sumatriptan. Headache 40:513–520

18. Lambert GA (2005) Preclinical neuropharmacology of naratriptan. CNS Drug Rev 11:289–316

19. Connor HE (2001) Building on the sumatriptan experience: the development of naratriptan. Cephalalgia 21:32–34

20. Adelman JU, Lipton RB, Ferrari MD, Diener HC, McCarroll KA, Vandormael K, Lines CR (2001) Comparison of rizatriptan and other triptans on stringent measures of efficacy. Neurology 57:1377–1383

21. Edvinsson L, Tfelt-Hansen P (2008) The blood–brain barrier in migraine treatment. Cephalalgia 28:1245–1258

22. Wood I, Pickholz M (2013) Concentration effects of sumatriptan on the properties of model membranes by molecular dynamics simulations. Eur Biophys J 42:833–841

23. Wojnar-Horton RE, Hackett LP, Yapp P, Dusci LJ, Paech M, Ilett KF (1996) Distribution and excretion of sumatriptan in human milk. Br J Clin Pharmacol 41:217–221

24. Imitrex Product Monograph (2013), Glaxo Smith-Kline, Brentford

25. Amerge Product Monograph (2014), Glaxo Smith-Kline, Brentford

26. Selivonchick DP, Roots BI (1977) Lipid and fatty acyl composition of rat brain capillary endothelia isolated by a new technique. Lipids 12:165–169

27. Fischer H, Gottschlich R, Seelig A (1998) Blood–brain barrier permeation: molecular parameters governing passive diffusion. J Membr Biol 165:201–211

28. Kalé L, Skeel R, Bhandarkar M, Brunner R, Gursoy A, Krawetz N, Phillips J, Shinozaki A, Varadarajan K, Schulten K (1999) NAMD2: greater scalability for parallel molecular dynamics. J Comp Physiol 151:283–312

29. Feller S, MacKerell AD Jr (2000) An improved empirical potential energy function for molecular simulations of phospholipids. J Phys Chem B 104:7510–7515

30. Jorgensen WL, Chandrasekhar J, Madura JD et al (1983) Comparison of simple potential functions for simulating liquid water. J Chem Phys 79:926–935

31. Martínez L, Andrade R, Birgin E, Martinez J (2009) PACKMOL: a package for building initial configurations for molecular dynamics simulations. J Comput Chem 30:2157–2164

32. Wood I, Martini MF, Pickholz M (2013) Similarities and differences of serotonin and its precursors in their interactions with model membranes studied by molecular dynamics simulation. J Mol Struct 1045:124–130

33. Becke A (1993) Density functional thermochemistry III The role of exact exchange. J Chem Phys 98:5648–5652

34. Frisch M, Trucks G, Schlegel H et al. (2003) Gaussian03, Revision B.05. Pople, Gaussian, Inc, 2003 Pittsburgh, PA.

35. Singh U, Kollman P (1984) An approach to computing electrostatic charges for molecules. J Comput Chem 5:129–145

36. Kim K, Jordan KD (1994) Comparison of density functional and MP2 calculations on the water monomer and dimer. J Phys Chem 9:10089–10094

37. Martyna GJ, Tobias DJ, Klein ML (1994) Constant pressure molecular dynamics algorithms. J Chem Phys 101:4177–4189

38. Feller S, Zhang Y, Pastor R, Brooks B (1995) Constant pressure molecular dynamics simulation: the Langevin piston method. J Chem Phys 103:4613–4621

39. Tuckerman M, Berne B, Martyna GJ (1991) Molecular dynamics algorithm for multiple time scales: systems with long range forces. J Chem Phys 94:6811–6815

40. Essmann U, Perera L, Berkowitz M, Darden T, Lee H, Pedersen L (1995) A smooth particle mesh Ewald method. J Chem Phys 103:8577–8593

41. Kučerka N, Liu Y, Chu N, Petrache NI, Tristram-Nagle S, Nagle JF (2005) Structure of fully hydrated fluid phase DMPC and DLPC lipid bilayers using X-ray scattering from oriented multilamellar arrays and from unilamellar vesicles. Biophys J 88:2626–2637

42. Marrink S-J, Berendsen HJC (1994) Simulation of water transport through a lipid membrane. J Phys Chem 98:4155–4168

43. Martini MF, Disalvo EA, Pickholz M (2012) Nicotinamide and picolinamide in phospholipid monolayers. Int J Quantum Chem 112:3289–3295

44. Mecozzi S, West A, Dougherty D (1996) Cation−π interactions in simple aromatics: electrostatics provides a predictive tool. J Am Ceram Soc 118:2307–2308

45. Petersen F, Jensen M, Nielsen C (2005) Interfacial tryptophan residues: a role for the cation-π effect? Biophys J 89:3985–3996

46. Barlow DJ, Thornton JM (1983) Ion-pairs in proteins. J Mol Biol 168:867–885

47. Kumar S, Nussinov R (1999) Salt bridge stability in monomeric proteins. J Mol Biol 293:1241–1255

48. Aliste MP, MacCallum JL, Tieleman DP (2003) Molecular dynamics simulations of pentapeptides at interfaces: salt bridge and cation−π interactions. Biogeosciences 42:8976–8987

49. Pascual J, Muñoz P (2005) Correlation between lipophilicity and triptan outcomes. Headache 45:3–6

50. Humphrey W, Dalke A, Schulten K (1996) VMD: visual molecular dynamics. J Mol Graph 14:33–38